Volume 12
Number 19
21 May 2024
Pages 6705–7112

Journal of Materials Chemistry C

Materials for optical, magnetic and electronic devices

rsc.li/materials-c

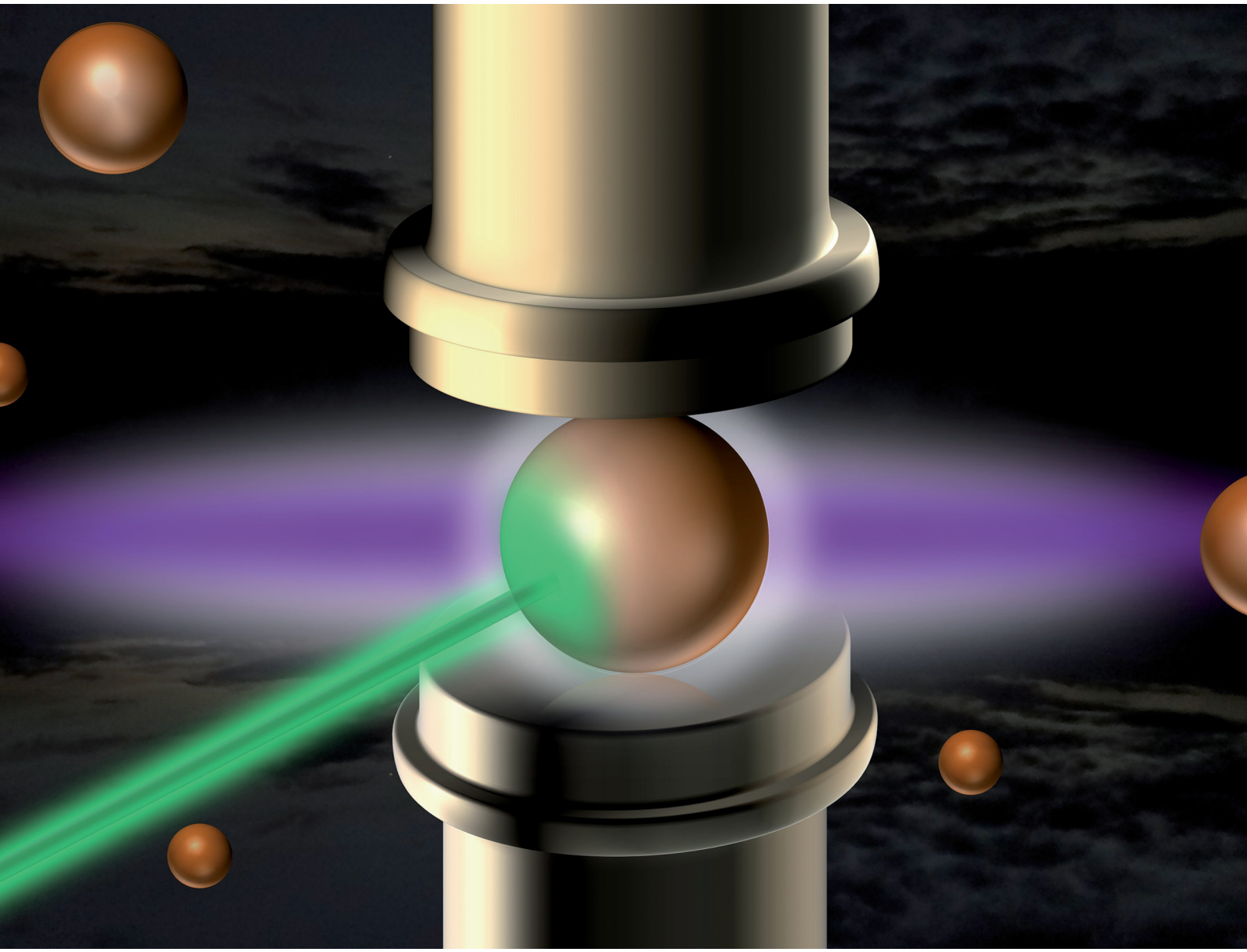

ISSN 2050-7526

ROYAL SOCIETY OF CHEMISTRY

PAPER

L. Marciniak *et al.*

A highly sensitive lifetime-based luminescent manometer and bi-functional pressure–temperature sensor based on a spectral shift of the R-line of Mn^{4+} in $K_2Ge_4O_9$

Journal of Materials Chemistry C

ROYAL SOCIETY OF CHEMISTRY

PAPER

View Article Online
View Journal | View Issue

Cite this: J. Mater. Chem. C, 2024, 12, 6793

A highly sensitive lifetime-based luminescent manometer and bi-functional pressure–temperature sensor based on a spectral shift of the R-line of Mn^{4+} in $K_2Ge_4O_9$†

M. Szymczak,[a] W. M. Piotrowski,[a] P. Woźny,[b] M. Runowski[b] and L. Marciniak*[a]

Although lifetime-based luminescent manometers exploiting the luminescence kinetics of Mn^{4+} ions exhibit remarkably attractive manometric performance, the number of studies reported in the literature devoted to this area is relatively small. Given that this type of manometer can exhibit very high sensitivity over a limited pressure range, in-depth studies on the correlation of the structure with the manometric properties of such pressure gauges are required to enable the design of manometers with predefined sensing performance. In response to these requirements, the present work investigates the spectroscopic properties of a new promising inorganic phosphor, *i.e.* $K_2Ge_4O_9$:Mn^{4+}, measured as a function of pressure and temperature. As is shown, the spectral shift of the Mn^{4+} R-line, the ratio of its emission intensity to phonon-progression bands, and the luminescence kinetics of the ^2E state can be used for remote pressure readout, with sensitivities of 0.59 nm GPa^{-1}, S_R = 21.7%/Gpa and 12%/Gpa, respectively. Notably, the developed manometer shows the highest sensitivity in the lifetime-based mode reported so far for pressure values above 2 Gpa. Furthermore, the considerable thermal sensitivity of the narrow emission line of Mn^{4+} ions (R-line) in the $K_2Ge_4O_9$:0.1% Mn^{4+} material, combined with its minimal shift under pressure for pressures below 1 GPa allows for the utilization of this phosphor as a luminescent sensor capable of concurrently measuring both pressure and temperature.

Received 29th December 2023,
Accepted 9th February 2024

DOI: 10.1039/d3tc04812h

rsc.li/materials-c

Introduction

The utilization of phosphors for the development of luminescent sensors has facilitated the remote readout of physical and chemical quantities with a high spatial resolution in an electrically passive manner.[1–9] As demonstrated by research in luminescence thermometry, among various spectroscopic parameters, two sensing modes, *i.e.* ratiometric and based on luminescence kinetics (lifetimes) offer the highest potential for imaging of physical quantities.[10–12] However, in the ratiometric mode, where the relative intensity variation of two emission bands is analyzed, the dispersive dependence of the extinction coefficient of the medium containing the phosphor or lying in the optical path between the phosphor and the detector, under specific conditions as well as the optical detection system, can bias the intensity ratio, leading to errors in the pressure readouts.[11] Therefore, an effective strategy often proposed in the literature is the use of sensors involving luminescence kinetics as a metrological parameter for diverse sensing purposes.[1,10,13–15] However, despite its attractiveness, this approach is modestly employed in luminescence manometry.[16–20] Pressure applied to the phosphor can induce various effects altering the luminescence kinetics of the emitting state, such as (I) phase transitions, resulting in a significant change in the energy level structure of the system; (II) formation of crystal defects, which may result in energy migration to traps and defect states; and (III) shortening the interionic distances, leading to increased probabilities of interionic energy transfer, which may induce nonradiative depopulation of emitting levels due to cross-relaxation processes.[21–24] A key example is SrF_2:Yb^{3+},Er^{3+} where growing pressure activates cross-relaxation, shortening the lifetimes of the $^2H_{11/2}$ and $^4S_{3/2}$ levels of Er^{3+} ions.[17] Similar effects can be observed for other systems doped with lanthanide ions.[25–28] However, it should be noted that temperature elevation enhances the probability of depopulation of excited levels through multiphonon processes. Hence, temperature and pressure changes

[a] Institute of Low Temperature and Structure Research, Polish Academy of Sciences, Okólna 2, 50-422 Wrocław, Poland. E-mail: l.marciniak@intibs.pl
[b] Adam Mickiewicz University, Faculty of Chemistry, Uniwersytetu Poznańskiego 8, 61-614 Poznań, Poland

† Electronic supplementary information (ESI) available. See DOI: https://doi.org/10.1039/d3tc04812h

in the system typically manifest in a very similar way in relation to the luminescence kinetics of lanthanide ions.[17] This not only introduces the possibility of deterioration in the reliability and credibility of sensing readouts but also hinders the measurement of pressure independently of temperature. Therefore, an alternative approach is necessary for the detection of pressure changes under extreme conditions. As a response to this demand lifetime-based luminescent manometers based on materials doped with transition metal (TM) ions have been recently proposed.[18,19,29–32] Due to the unique electronic configuration of TM ions, their spectroscopic properties exhibit high sensitivity to the changes in the local environment of the ions. In general, the compression of the phosphor induces a change in the strength of the crystal field acting on these ions. This is particularly evident for ions with a $3d^3$ electronic configuration (*e.g.*, Cr^{3+}, Mn^{4+}), where pressure growth boosts the crystal field strength, elevating, among others, the energy of the $^4T_2$ energy level. Due to the spin–orbit coupling between the ^2E and $^4T_2$ levels, the energy increase of the $^4T_2$ level reduces the coupling strength, leading to the prolongation of the lifetime of the ^2E level. The observed prolongation of the lifetime is a unique effect that distinguishes this type of luminescent manometer from other lifetime-based pressure gauges. Importantly, for most phosphors doped with Mn^{4+} ions, the high activation energy of nonradiative depopulation of the ^2E level renders the luminescence kinetics associated with the $^2E \rightarrow {}^4A_2$ electronic transition insensitive to temperature changes at room temperature. While the theoretical foundations of this solution seem particularly attractive from an application perspective, they have not been extensively explored in the literature to date.[18,19]

Therefore, this study presents a comprehensive analysis of the spectroscopic properties of $K_2Ge_4O_9$:Mn^{4+} as a function of pressure and temperature to evaluate its application potential for remote pressure and temperature sensing. The performed analysis enables the selection of the optimal dopant concentration to obtain intense emission and a long lifetime of the ^2E state. The high-pressure spectroscopy analysis indicates that the spectral and temporal luminescence properties of the $K_2Ge_4O_9$:Mn^{4+} material are significantly affected by pressure. Therefore, the spectral shift, luminescence intensity ratio, and lifetime-based approaches to luminescence manometry were investigated and their thermal sensitivities were analyzed. Moreover, utilizing the unprecedentedly large, temperature-induced spectral shift of the ultra-narrow emission band of Mn^{4+} (R-line), and its negligible pressure-dependence in the low-pressure range, we were able to develop a truly bifunctional manometer-thermometer operating under extreme conditions.

L. Marciniak

Lukasz Marciniak (prof. in physics) received his PhD and habilitation in Physics at the Institute of Low Temperature and Structure Research, Polish Academy of Sciences (ILTSR PAS), in 2014 and 2017, respectively. In 2022 he become a full professor. He is the co-author of more than 200 publications and 12 patents. His current research focuses on the luminescence properties of advanced multifunctional materials with a special emphasis on their application in remote sensing and imaging of physical and chemical parameters i.e. temperature (luminescent thermometer), pressure (luminescent manometry) and pH. He conducts interdisciplinary scientific research on the borders of physics, chemistry, chemical engineering, material engineering, and biology.

Experimental

$K_2Ge_4O_9$ powders doped with different concentrations of Mn^{4+} were obtained by using the solid-state synthesis method. Germanium oxide (GeO_2; 99.999% purity; from Sigma Aldrich) and manganese(II) chloride tetrahydrate ($MnCl_2{\cdot}4H_2O$; 99% purity; from Sigma Aldrich) were used in stoichiometric amounts. On the other hand, potassium carbonate (K_2CO_3; 99.997% purity; from Alfa Aesar) was used in a 20% excess. The raw materials were ground in an agate mortar with hexane, transferred to porcelain crucibles and annealed at 1123 K for 6 hours under an air atmosphere. The obtained materials were then examined by X-ray powder diffraction (XRD) using a PANalytical X'Pert Pro diffractometer in Bragg–Brentano geometry equipped with an Anton Paar TCU1000 N temperature control unit using Ni-filtered Cu K α radiation (V = 40 kV, I = 30 mA). Measurements were performed in the range of 10–90°. Transmission electron microscopy (TEM) images were taken using a Philips CM-20 SuperTwin microscope. The samples were dispersed in methanol, and a drop of prepared suspension was put on a copper grid. Next, the samples were dried and purified in a plasma cleaner. Studies were performed in a conventional TEM procedure with a parallel beam electron energy of 1160 kV. The size of the obtained powders was determined manually using ImageJ software by measuring the longest linear size (Feret diameter) of each particle. The $K_2Ge_4O_9$ material was investigated by Raman spectroscopy in the pressure range from ≈0 to 10 GPa, in a backscattering geometry using a Renishaw inVia confocal micro-Raman system with a power-adjustable 100 mW 532 nm laser. An optical system with an Olympus x20 SLMPlan N long working distance objective was used to focus the laser beam. Vibrational analysis for the sample compressed in a pressure transmitting medium (methanol : ethanol : water – 16 : 3 : 1) was conducted in a diamond anvil cell (DAC) equipped with the ultra-low fluorescence diamond anvils (IIas type). Excitation and emission spectra were measured on an FLS1000 spectrometer from Edinburgh Instruments supplied with a 450 W xenon lamp as an excitation source, and the R928P side window photomultiplier tube from Hamamatsu as a detector. The emission spectra and

luminescence decay profiles as a function of pressure and temperature were measured using the same system with a 445 nm laser diode as the excitation source. A THMS 600 heating–cooling stage from Linkam was utilized to control the temperature with a precision of 0.1 K. Pressure-dependent luminescence studies were conducted in a gas (nitrogen) membrane-driven diamond anvil cell Diacell μScopeDAC-RT(G) from Almax easyLab with a 0.4 mm diamond culets. The sample and pressure indicator Al_2O_3:Cr^{3+} were placed in a ≈140 μm hole drilled in a 250 μm thick stainless-steel gasket. The pressure transmission medium was methanol : ethanol : water – (16 : 3 : 1).

A Druck PACE 5000 was used to control the applied pressure. Accurate determination of the pressure in the DAC was possible by controlling the spectral shift of the R1 ruby (Al_2O_3:Cr^{3+}) line.

Results and discussion

The $K_2Ge_4O_9$ crystallizes in a trigonal structure with *P*3*c*1 space group (No. 165) with lattice parameters a = 11.84, b = 11.84 and c = 9.8 (Å).[33–36] The structure of the $K_2Ge_4O_9$, similarly like in the case of the family of tetragermanates of alkali ions, consists of characteristic Ge_3O_9 rings that form layers in the *ab* planes (Fig. 1a). As it can be seen, there are four nonequivalent Ge sites in the structure, *i.e.* two tetrahedral (Ge(2) and Ge(3)) and two octahedral (Ge(1) and Ge(4)). The Ge_3O_9 rings consist of two $Ge(3)O_4$ and one $Ge(2)O_4$ thus created planes are connected by each other through two types of $Ge(1)O_6$ and $Ge(2)O_6$ octahedra by sharing O^{2-} ions. Due to the size and the preferred coordination only octahedral sites can be occupied by the Mn^{4+} ions. Therefore only Ge(1) and Ge(4) can be considered as potential sites replaced by the dopant ions in the $K_2Ge_4O_9$ structure. As calculated by Redhammer *et al.* the Ge(4) is a bit smaller than Ge(1), and in contrast to the Ge(4), the Ge(1) site exhibits inversion symmetry.[35,37] Therefore it is expected that the emission spectra of $K_2Ge_4O_9$:Mn^{4+} will be dominated by the signal of the Mn^{4+} from the low-symmetry Ge(4) site. Based on the XRD data it was found that in the case of the stoichiometric amounts of the reagents due to the lability of K^+ ions, additional reflections were found in the diffractograms revealing the presence of the GeO_2 phase (Fig. 1b). The intensity of those reflections decreases gradually with the enlarging concentration of the excessing K_2CO_3 and finally for the 20% molar excess the pure $K_2Ge_4O_9$:Mn^{4+} powders were obtained. Therefore this reactant molar ratio was used for further synthesis.

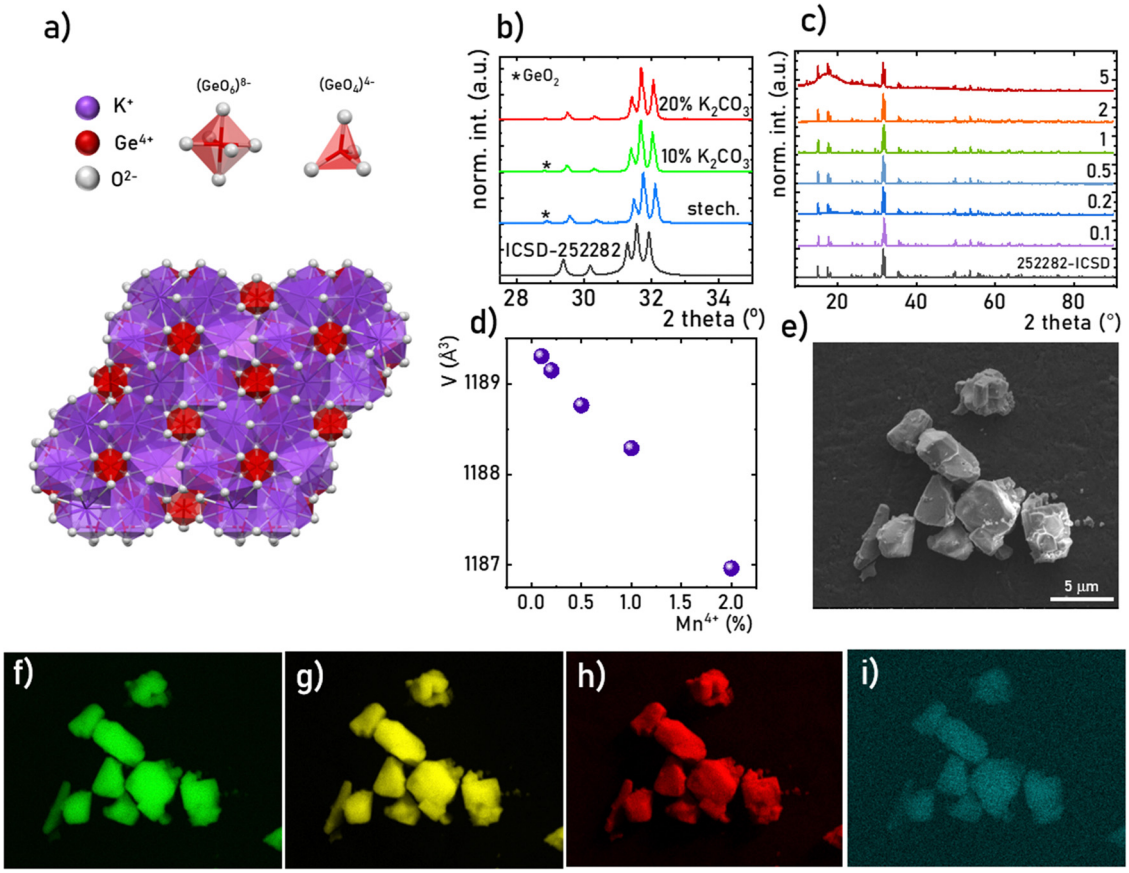

Fig. 1 Visualization of the $K_2Ge_4O_9$ structure (a), XRD patterns of the $K_2Ge_4O_9$:Mn^{4+} for different molar excess of K_2CO_3 (b), comparison of XRD patterns of the $K_2Ge_4O_9$:Mn^{4+} for different concentration of Mn^{4+} ions (c), the volume of the unit cell of the $K_2Ge_4O_9$:Mn^{4+} as a function of Mn^{4+} concentration determined from Rietveld refinement (d), representative SEM image of the $K_2Ge_4O_9$:0.1%Mn^{4+} (e), and corresponding EDS maps of the elemental distribution of K (f), Ge (g), O (h) and Mn (i).

The analysis of the XRD patterns obtained for different concentrations of Mn^{4+} ions indicates the lack of additional X-ray reflexes confirming the phase purity of the obtained materials (Fig. 1c). However, in the case of the sample with 5% of Mn^{4+} ions, some broad band at low 2-theta angles was observed in the XRD pattern, most probably indicating the partial amorphization of the $K_2G_4O_9$ structure. Therefore the analysis discussed in this paper was limited to the 0.1–2% Mn^{4+} dopant concentration. Based on the Rietveld refinement of the obtained XRD patterns, the unit cell volume was determined as a function of the Mn^{4+} concentration. The contraction of the cell volume, resulting from the difference in the ionic radii between Ge^{4+} and Mn^{4+} ions, confirms the successful replacement of host cations by the dopant ions (Fig. 1d, see Table S1 for Rietveld refinement parameters, ESI†). The SEM images reveal that the obtained powders consist of aggregated particles of average size around 2.5 μm in diameter (Fig. 1e), whereas the EDS spectroscopy validates the uniform distribution of all constituent ions and dopant ions (Fig. 1f–i).

The structural stability of the investigated $K_2Ge_4O_9$ material was analyzed by measuring the Raman scattering spectra with pressure. The recorded spectrum for the investigated material at 0.46 GPa (initial pressure value obtained in a DAC) has seven bands initially located around ≈240 and 400-internal vibrations, 515, 535 and 565 – the symmetric bending vibration of Ge–O–Ge, 820 and 900 cm^{-1} – the symmetric stretching vibration of Ge–O–Ge (Fig. 2a and b). Under the compression process (increasing pressure in the system) the energies of all phonon modes increase, and the Raman modes centroids shift toward higher wavenumbers in the vibrational spectra, as shown in Fig. 2b. The calculated Raman mode spectral shifts with pressure are gradual and linear, which confirms the stability of the crystal structure of the investigated materials. The most intense Raman mode at ≈515 cm^{-1} shows the highest value of linear shift around 5.70 cm^{-1} GPa^{-1}. The calculated shift rates (cm^{-1} GPa^{-1}) for the observed Raman modes are gathered in Table S1 (ESI†). The observed effects are the results of the decrease of the interatomic distances in the structures under compression, *i.e.* bond shortening. Additionally, some changes in the Raman modes intensity ratio (between ≈3.5–5.5 GPa), as well as the vanishing and emerging of the corresponding two peaks (at around ≈560 cm^{-1}) were observed. This effect may indicate a gradual pressure-induced phase transition of the $K_2Ge_4O_9$ material, which is reversible, as confirmed by decompression data. The high signal-to-noise ratio for all measured Raman spectra (even under extreme values of high pressure) is related to the very good crystallinity of the $K_2Ge_4O_9$ material. It may also indicate that crystal defects and strains, which are typically observed during high-pressure Raman measurements, do not play a significant role during the compression process in this case, for this particular material. Moreover, in the decompression cycle, the reverse tendencies of spectral shift and the shape of Raman modes were observed, namely, they fully come back to the initial state upon pressure

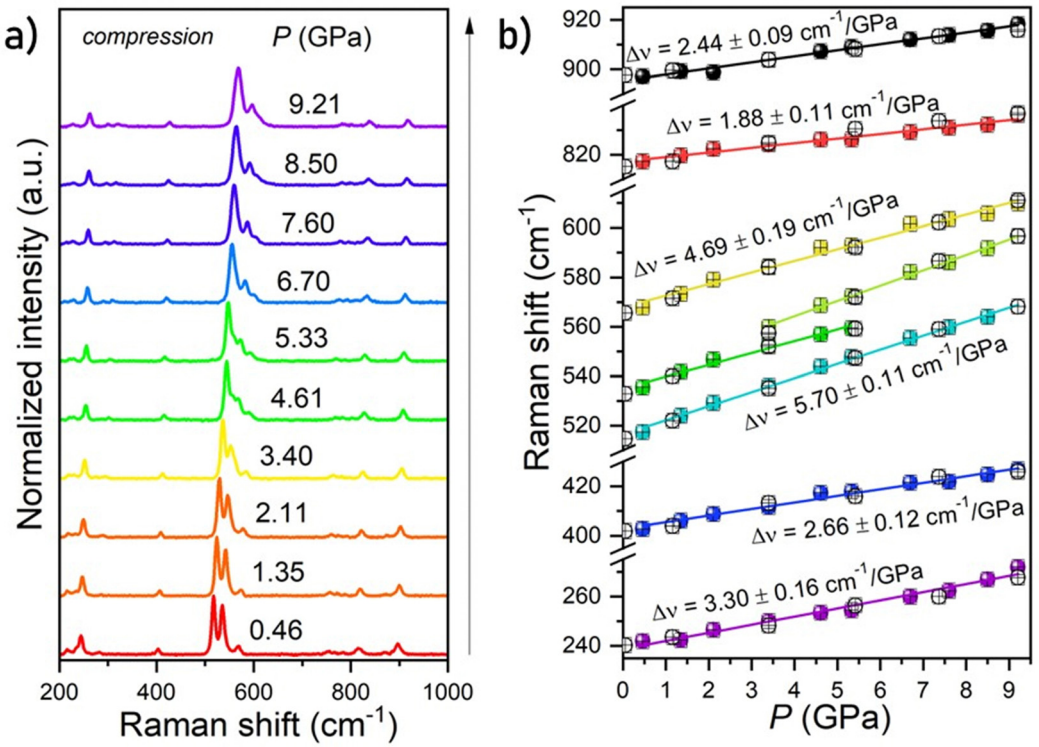

Fig. 2 Normalized Raman spectra for the $K_2Ge_4O_9$ material in the compression process (a). Calculated peak centroids of phonon modes under compression (b); spheres present peak centroid values in compression, empty circles represent peak centroids in the decompression process; the lines are the linear function fitted for determination of the pressure-induced shift rates of the Raman modes.

release (see Fig. 2b and Fig. S1, ESI†). In other words, no plastic deformations during the compression–decompression cycle were observed. The same position of initial Raman modes before compression and after the decompression cycle is evidence of reversibility of the whole compression process, including structural changes and phase transition in the $K_2Ge_4O_9$ material. This factor is an important aspect in designing new optical manometers, so the examined $K_2Ge_4O_9$ material might be considered as a potential contactless pressure sensor.

Mn^{4+} ions are well-known in the literature and are often used as luminescent dopants providing the possibility of generation of deep-red emission. The luminescence properties of these ions are related to the spin-forbidden $^2E \rightarrow {}^4A_2$ electronic transition. The ^2E level, unlike the $^4T_2$ and $^4T_1$ levels due to the absence of a shift of its parabola in the wavevector domain with respect to the $^4A_2$ ground state, is located directly above the bottom of the $^4A_2$ level. Therefore, the radiative transition between ^2E and $^4A_2$ is represented in the emission spectra as a spectrally narrow band, often accompanied by lines associated with phonon progression (Fig. 3a). In the case of the $K_2Ge_4O_9$ compound, the $^2E \rightarrow {}^4A_2$ emission band is located at around 670 nm (R line at 650 nm), and its shape is independent of the dopant ion concentration (Fig. 3b). The excitation spectrum of the $K_2Ge_4O_9$:Mn^{4+} consists of a group of spectrally broad bands located in the range of 260–563 nm (38 532–17 746 cm^{-1}). The deconvolution of the excitation spectrum allows to indicate the maxima of these bands: $^4A_2 \rightarrow {}^4T_2$ (21 920 cm^{-1}), $^4A_2 \rightarrow {}^2T_2$ (24 795 cm^{-1}); $^4A_2 \rightarrow {}^4T_1$ (29 320 cm^{-1}) and $Mn^{4+} \rightarrow O^{2-}$ charge transfer band (33 527 cm^{-1}) (Fig. 3c). An increase in temperature results in a gradual thermalization of higher lying vibrational states of the ^2E level, until the delivered thermal energy is sufficient to exceed the intersection point between the ^2E and $^4T_2$ states, resulting in nonradiative depopulation of the ^2E level. The relatively large value of the energy of this crossover point (usually >1000 cm^{-1})[38] results in the high thermal stability of Mn^{4+} luminescence. The energies of the ^4T_J states are strongly dependent on the crystal field strength affecting the Mn^{4+} ions. Therefore, the compression of the host material by applied external pressure causes the increase of energy of ^4T_J inducing all the associated spectroscopic consequences discussed later in this paper. Although the shape of the emission spectrum changes negligibly with varying concentrations of dopant ions, the intensity of the luminescence decreases significantly (Fig. 3d). The maximum luminescence intensity is observed for the sample with 0.1% of Mn^{4+} (exceeding twice the intensity of luminescence obtained for the one with 0.2% of Mn^{4+}). Therefore, this dopant ion concentration was used for high-pressure research. The analysis of the luminescence kinetics revealed that as the dopant ion concentration increases, the luminescence decay profiles from the ^2E level deviate from the exponential character (luminescence decay curve can be found in Fig. S3, ESI†). Therefore, in order to provide a comparative analysis of the effect of dopant ion concentration on the lifetime of the ^2E level, the average lifetimes were determined using (eqn (1)) based on parameters obtained by fitting the measured luminescence decay profiles to the double exponential function (eqn (2)).

$$\tau_{avr} = \frac{A_1\tau_1^2 + A_2\tau_2^2}{A_1\tau_1 + A_2\tau_2}. \quad (1)$$

$$I(t) = I_0 + A_1 \cdot \exp\left(-\frac{t}{\tau_1}\right) + {}_1 \cdot A_2 \exp\left(-\frac{t}{\tau_2}\right). \quad (2)$$

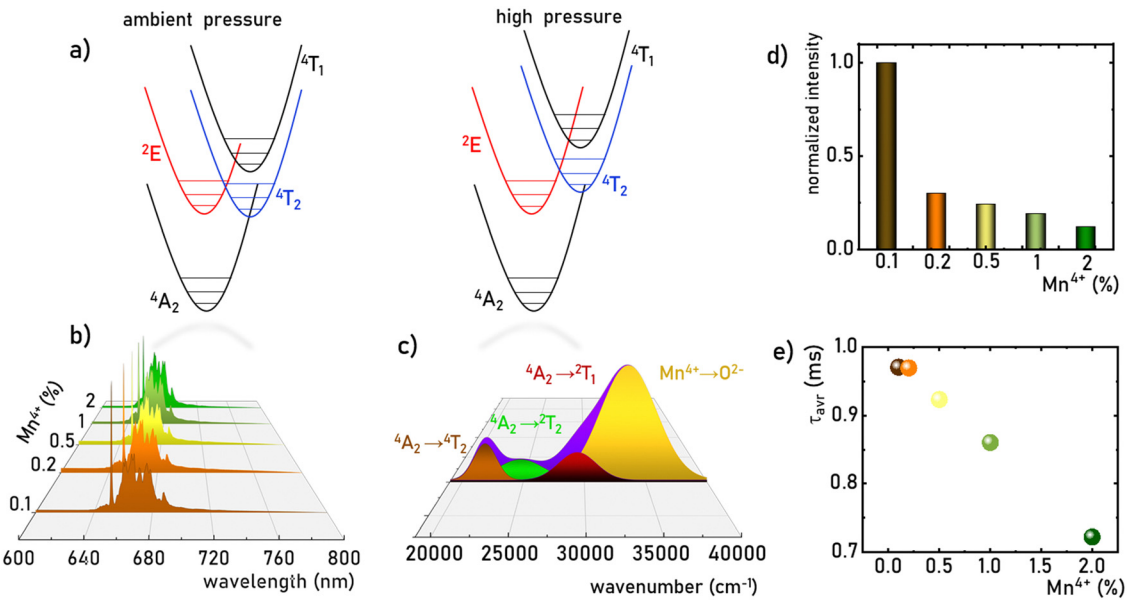

Fig. 3 The simplified configurational coordination diagram of Mn^{4+} ions at ambient and high-pressure conditions (a); the comparison of the normalized emission spectra of the $K_2Ge_4O_9$:Mn^{4+} measured at 83 K upon λ_{exc} = 445 nm for different Mn^{4+} concentration (b); the deconvolution of the excitation spectrum of the $K_2Ge_4O_9$:0.1%Mn^{4+} sample measured at 83 K for λ_{em} = 651 nm (c); comparison of the integrated emission intensity of the $K_2Ge_4O_9$:Mn^{4+} samples at room-temperature (d) and τ_{avr} (e) as a function of the Mn^{4+} concentration.

where A_1, A_2, τ_1 and τ_2 are the fitting parameters. The analysis showed that for the concentrations of 0.1–0.2% of Mn^{4+} the τ_{avr} = 0.98 ms, and shortens linearly with increasing concentration of Mn^{4+} ions, reaching 0.71 ms at 2% of Mn^{4+}.

The Mn^{4+} ions with the $3d^3$ electronic configuration similarly to Cr^{3+} ions are extremely sensitive to changes in the strength of the crystal field. Therefore, the applied pressure (leading to the contraction of the unit cell and consequent shortening of the Mn^{4+}–O^{2-} distances) increases the strength of the crystal field acting on Mn^{4+} ions. A careful analysis of the Tanabe–Sugano diagram for ions of $3d^3$ configuration indicates that such a change in the strength of the crystal field leads to an increase in the energy of ^4T_J levels. In contrast, the energy of the ^2E state reveals the independence of the changes in the strength of the crystal field. However, shortening the Mn^{4+}–O^{2-} distance enhances the covalency of this bond, which, in turn, through the nephelauxetic effect, slightly decreases the energy of the ^2E level, resulting in a red-shift of the $^2E \rightarrow {}^4A_2$ band with pressure (Fig. 4a, see also Fig. S4, ESI†). This is an effect commonly used for pressure sensing in the case of the well-known ruby (Al_2O_3:Cr^{3+}) sensor. In the case of the $K_2Ge_4O_9$:Mn^{4+}, the applied pressure leads to a shift of the R-line from 15 332 cm^{-1} at ambient pressure to 15 238 cm^{-1} at 7.6 GPa. In addition, as can be seen in Fig. 4a, an increase in pressure results in a broadening of emission lines and a reduction in their emission intensity. Although the data presented in Fig. 4a are normalized, an increase in noise-to-signal ratio as pressure increases can be recognized. A decrease in emission intensity with increasing pressure is very common in high-pressure spectroscopy, and in this case it may result from a growing number of strains and defect states that act as quenching centers, as well as from improved cross-relaxation processes in a compressed structure. A detailed analysis of the excitation spectra of Mn^{4+} ions shows, as expected, an increase in the energy of the bands associated with the $^4A_2 \rightarrow {}^4T_i$ transitions (Fig. 4b). The observed change in band energies

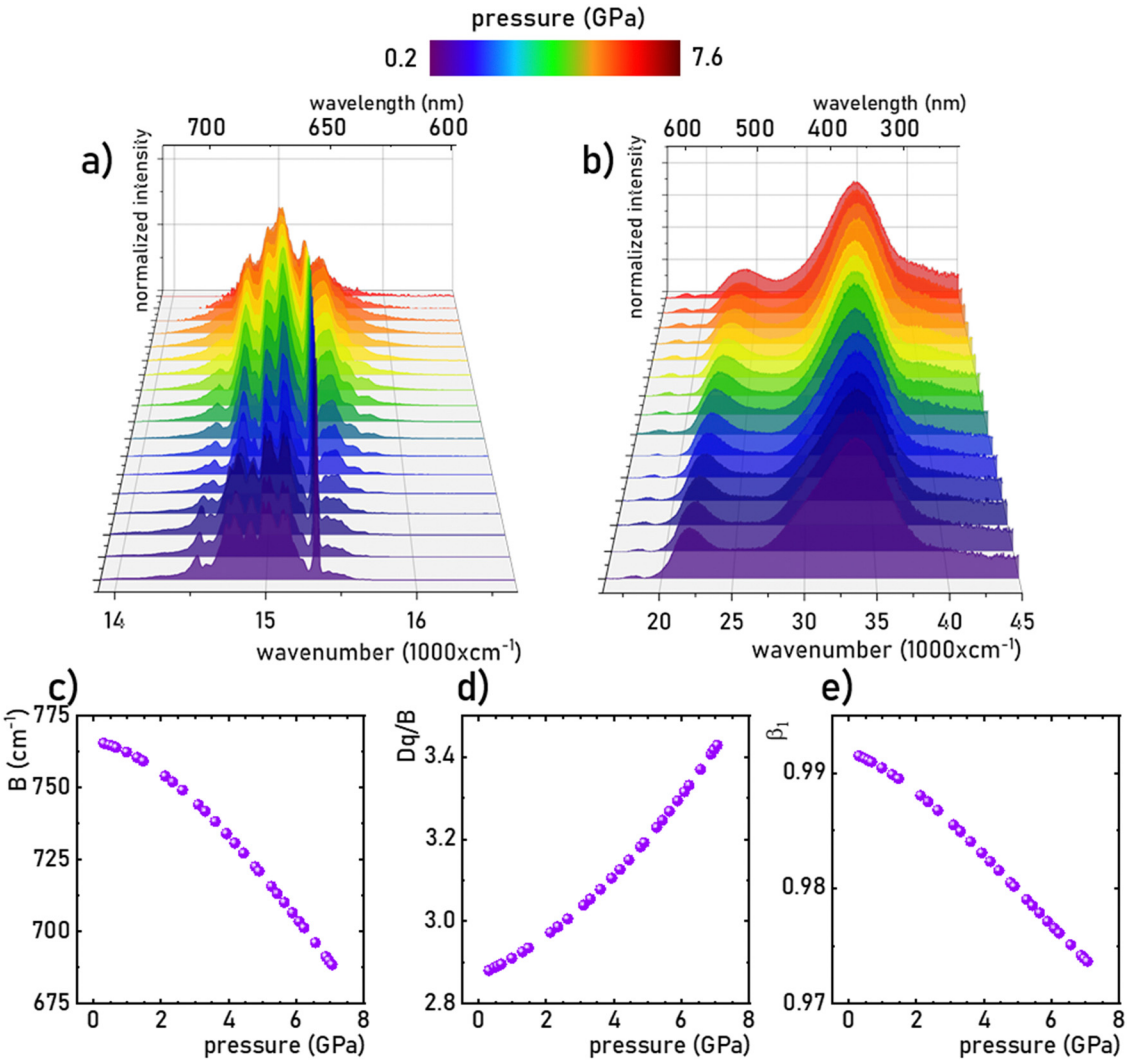

Fig. 4 The normalized room-temperature emission spectra (λ_{exc} = 445 nm) of the $K_2Ge_4O_9$:0.1%Mn^{4+} material (a) and excitation spectra (λ_{em} = 651 nm) (b) measured as a function of applied pressure, and the corresponding B (c), Dq/B (d) and β_1 (e) parameters calculated based on the excitation spectra.

amounted to 1987 cm^{-1} (from 21 964 cm^{-1} at ambient pressure to 23 951 cm^{-1} at 7.6 GPa) for the $^4A_2 \rightarrow {}^4T_2$ band and 1326 cm^{-1} (from 33 654 cm^{-1} at ambient pressure to 34 980 cm^{-1} at 7.6 GPa) for the $^4A_2 \rightarrow {}^4T_1$ band. The data obtained allowed the determination of the crystal field Dq and Racah B and C parameters as follows:[39–41]

$$E(^4A_2 \rightarrow {}^4T_2) = 10Dq \quad (3)$$

$$\frac{Dq}{B} = \frac{15\left(\frac{\Delta E}{Dq} - 8\right)}{\left(\frac{\Delta E}{Dq}\right)^2 - 10\frac{\Delta E}{Dq}} \quad (4)$$

$$\frac{E(^2E \rightarrow {}^4A_2)}{B} = \frac{3.05C}{B} + 7.9 - \frac{1.8B}{Dq} \quad (5)$$

As observed, the B parameter gradually decreases with pressure, which is a typical effect observed for materials doped with Mn^{4+} ions (Fig. 4c, for pressure dependence of C parameter see Fig. S5, ESI†).[38,42,43] Its value at ambient pressure equals 757 cm^{-1}, which corresponds to relatively high values of crystal field strength. On the other hand, the Dq/B parameter increases significantly with pressure, *i.e.* from 2.85 at ambient pressure to about 3.47 at 7.6 GPa (Fig. 4d). The nephelauxetic effect as proposed by Brik *et al.* can be analyzed through parameter β_1 defined as follows:[44,45]

$$\beta_1 = \sqrt{\frac{B}{B_0} + \frac{C}{C_0}} \quad (6)$$

where B_0 and C_0 are the values for free ions equal to 1160 and 4303 cm^{-1}, respectively.[45] An increase in the covalency of the Mn^{4+}–O^{2-} bond is confirmed by a monotonic decrease in the B_1 parameter with increasing pressure (Fig. 4e). Notably, the observed reduction in the B_1 parameter is greater (1.9% change) than for the recently reported $Sr_4Al_{14}O_{25}$:Mn^{4+} material (0.25% change in the analogous pressure range).[18]

The monotonic change in the energy maximum of the $^2E \rightarrow {}^4A_2$ band or the corresponding change in the spectral position of this band as a function of the applied pressure makes it possible to develop a spectral-shift based luminescence manometer. It can be clearly seen that in the analyzed pressure range, a change in the energy of the ^2E level of about 80 cm^{-1} is observed, which corresponds to a change in the spectral position of the band of about 3 nm (Fig. 5a). Quantitative analysis of the spectral band shift is usually done by determining the absolute sensitivity ($S_{A,p}$) as follows:

$$S_{A,p\,(cm^{-1})} = \frac{\Delta E}{\Delta p} \quad (7)$$

$$S_{A,p\,(nm)} = \frac{\Delta \lambda}{\Delta p} \quad (8)$$

In the case of the $K_2Ge_4O_9$:0.1%Mn^{4+} phosphor, the value of $S_{A,p}$ increases with pressure up to about 5 GPa, at which point $S_{A,p}$ reaches a maximum ($S_{A,p(cm^{-1})}$ = 12 cm^{-1}/GPa; $S_{A,p(nm)}$ = 0.59 nm GPa^{-1}). Beyond this pressure, a decrease in $S_{A,p}$ is observed (Fig. 5b). The sensitivity values obtained for the $K_2Ge_4O_9$:0.1%Mn^{4+} material fall within the typical range of spectral shifts observed for transition metal ions with a $3d^3$ electronic configuration when emission occurs from the ^2E level. Importantly, the achieved $S_{A,p}$ value exceeds the sensitivity of the ruby sensor – Al_2O_3:Cr^{3+} ($S_{A,p}$ = 0.365 nm GPa^{-1}).[46] For real-world applications, a change in pressure may be accompanied by a change in the temperature of the analyzed object. Therefore, low sensitivity to temperature changes of the luminescent manometer is essential to maintain high reliability of pressure value determination. For this purpose, emission spectra of $K_2Ge_4O_9$:0.1%Mn^{4+} were measured as a function of temperature (Fig. 5c) the thermal sensitivity of the

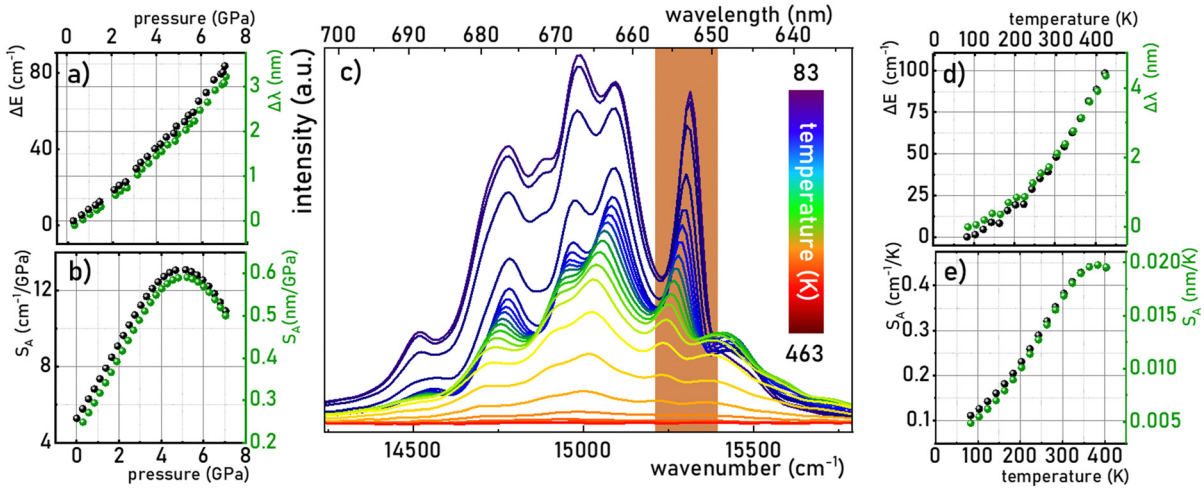

Fig. 5 Change in the energy and wavelength of the R line of the $^2E \rightarrow {}^4A_2$ emission band maxima as a function of pressure (a) and corresponding S_A (b); emission spectra of $K_2Ge_4O_9$:0.1%Mn^{4+} measured as a function of temperature at ambient pressure (λ_{exc} = 445 nm) (c) thermal dependence of the change in the energy and wavelength of the R line of the $^2E \rightarrow {}^4A_2$ emission band maxima (d) and corresponding S_A (e).

manometer is analyzed, determined in a manner analogous to $S_{A,p}$:

$$S_{A,T\,(cm^{-1})} = \frac{\Delta E}{\Delta T} \quad (9)$$

$$S_{A,T_{(nm)}} = \frac{\Delta \lambda}{\Delta T} \quad (10)$$

An increase in temperature causes a successive decrease in the intensity of the $^2E \rightarrow {}^4A_2$ emission associated with the thermalization of the $^4T_2$ level, followed by nonradiative transitions to the $^4A_2$ ground state. Consequently, the luminescence intensity at 423 K is low. Therefore, the analysis was limited to the 83–423 K range. In this temperature range, a gradual shift in the energy of this energy level of about 100 cm^{-1} (4 nm) was observed (Fig. 5d), which corresponds to the $S_{A,T}$ of 0.45 cm^{-1} K^{-1} (0.02 nm K^{-1}), as shown in Fig. 5e. This is almost three times higher than that observed for $Al_2O_3:Cr^{3+}$ ($S_{A,T}$ = 0.007 nm K^{-1}),[47,48] which reduces the reliability of the pressure reading using the spectral shift of the emission band of Mn^{4+} ions in the $K_2Ge_4O_9$:0.1%Mn^{4+}.

However, it is noteworthy that a pronounced thermal shift in the spectral position of the R-line (which is very narrow) associated with Mn^{4+} ions is exceptionally rare, rendering it an exceedingly precise temperature indicator. While literature commonly discusses the spectral shift of a band as a parameter of limited utility for temperature imaging, given the necessity for point-by-point measurements across emission spectra, a single-point reading of such a spectrally narrow line, exhibiting high sensitivity to temperature variations, proves highly advantageous for other (than imaging) temperature monitoring purposes. This capability facilitates accurate temperature determination without the need for measurements across a wide spectral range. The dual sensitivity of the same parameter to both temperature and pressure changes may be perceived as a potential limitation in sensor applications. However, it is pertinent to note that within the pressure range typically employed in most industrial applications (up to $\sim 10^{-1}$ GPa), the pressure-induced shift of the R-line is merely 0.4 cm^{-1}. In contrast, within the analyzed temperature range, a thermal shift exceeding 100 cm^{-1} is observed. The pressure sensitivity of the spectral position of the Mn^{4+} emission band in $K_2Ge_4O_9$:0.1%Mn^{4+} is significantly lower compared to other already reported Mn^{4+} luminescence manometers like Gd_2ZnTiO_6 of 1.11 nm GPa^{-1} sensitivity in the spectral shift readout mode.[49] Consequently, $K_2Ge_4O_9$:0.1%Mn^{4+} can be effectively employed as a bi-function sensor capable of concurrently measuring temperature and pressure under extreme conditions, showcasing its versatility and utility across diverse applications.

Although spectral shift is the most commonly used spectroscopic parameter for luminescent pressure sensors, its use is difficult or impossible in certain applications. Imaging pressure changes over a larger area (*via* 2D/3D mapping) using spectral-shift based manometers would be very time consuming, as requiring point-by-point measurement of emission spectra. Therefore, an alternative strategy reported recently in the literature is the ratiometric approach, in which the ratio of luminescence intensities in two spectral regions (LIR) is a manometric parameter.

The analysis of the $K_2Ge_4O_9$:0.1%Mn^{4+} emission spectra as a function of pressure indicates that the R-line not only undergoes a spectral shift, but also decreases in intensity with respect to the lines associated with phonon progression. Therefore, the LIR is defined as follows:

$$LIR = \frac{\int_{649nm}^{656nm} {}^2E \rightarrow {}^4A_2 d\lambda}{\int_{673nm}^{680nm} {}^2E \rightarrow {}^4A_2 d\lambda} \quad (11)$$

shows high variability as a function of pressure (in the wavenumber domain the LIR can be calculated in the following regions 15 243–15 408 cm^{-1}/14 858–14 706 cm^{-1}). As presented in Fig. 6a the maximum value was reached at about 3 GPa, and then the LIR parameter decreased monotonically with further pressure increase. The value of the pressure at which the maximum sensitivity was reached correlates well with the pressure value above which some changes in the vibronic spectra were found. Therefore probably the changes in the S_R are associated with the structural changes of the host material. However, the measurement during the compression–decompression cycles confirmed that observed changes are reversible. Therefore, the relative sensitivity ($S_{R,p}$) is defined as follows:

$$S_{R,p} = \frac{1}{LIR}\frac{\Delta LIR}{\Delta p}100\% \quad (12)$$

reaches negative values in the pressure range below 3 GPa, and increases with pressure up to 5.9 GPa, at which point $S_{R,p}$ = 21.7%/GPa was obtained (Fig. 6b). Of course, the negative S_R values are only due to the conventions of LIR calculation. However, changing the monotonicity of the gauge operating parameter strongly limits the useful range of pressure values over which it can be used, because otherwise one LIR value would correspond to two different pressure values making the gauge useless. Therefore, it should be clearly underlined here that for $K_2Ge_4O_9$:0.1%Mn^{4+} the LIR can be used as a sensing parameter for pressure above 3 GPa. Importantly the thermal relative sensitivity is defined by analogy to pressure sensitivity:

$$S_{R,T} = \frac{1}{LIR}\frac{\Delta LIR}{\Delta T}100\% \quad (13)$$

reaches values of about $S_{R,T}$ = 1.3%/GPa around 140 K, and above 200 K it drops almost to zero (Fig. 6d), which confirms the higher thermal invariability of LIR sensing mode (Fig. 6c) compared to a manometer based on the spectral shift. A quantitative manifestation of the thermal invariability of the manometer parameter to pressure changes is provided by the determination of the TIMF parameter (thermal invariability manometric factor) defined as follows:[29]

$$TIMF = \frac{S_{R,p}}{S_{R,T}} \quad (14)$$

The TIMF parameter determines how much change in absolute temperature (in K) is required to modify the value of

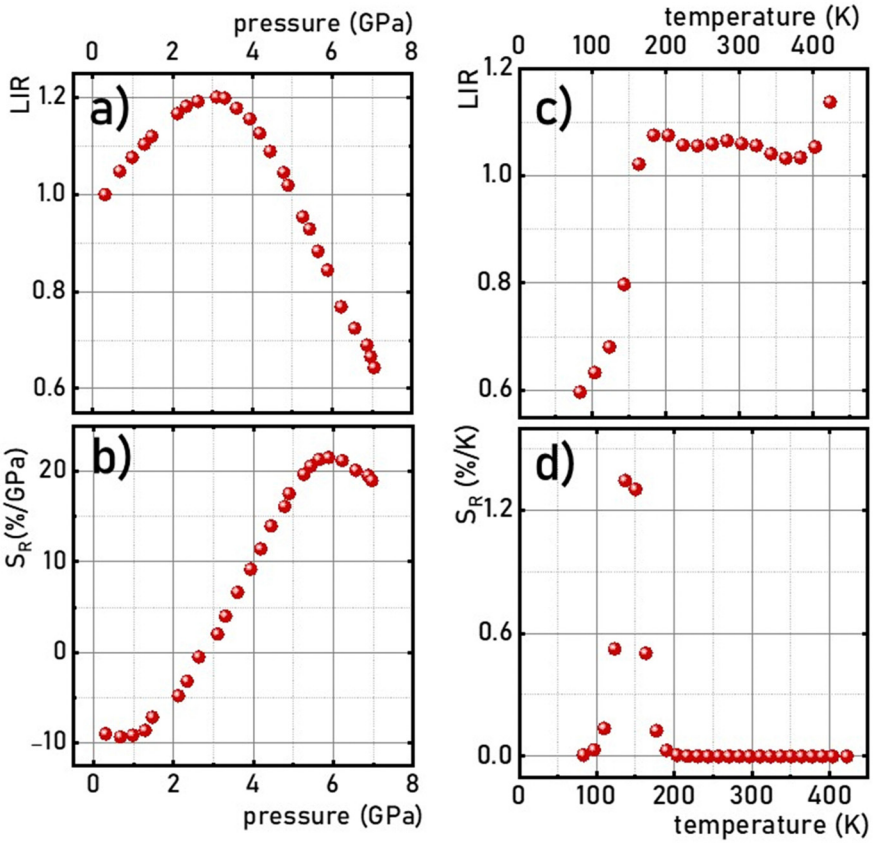

Fig. 6 Pressure –(a) and thermal –(b) dependences of the LIR and corresponding S_R- (c) and (d), respectively, in $K_2Ge_4O_9$:0.1%Mn^{4+}.

the manometric parameter corresponding to the change in pressure by 1 GPa. Ideally, for a luminescent pressure gauge that is insensitive to temperature changes, the TIMF should approach infinity. However, technically, it can be assumed that the manometer reveals adequate insensitivity to temperature changes when TIMF > 100[29]. Since thermal sensitivity depends on temperature, it is recommended to determine the TIMF in the operating temperature of the manometer, which in this case is around 300 K. In the case of the $K_2Ge_4O_9$:0.1%Mn^{4+} sensor operating in the ratiometric mode the TIMF = 5425 K/GPa ($S_{R,T}$@300 K = 0.004%/K), which indicates high reliability of $K_2Ge_4O_9$:0.1%Mn^{4+} as a ratiometric luminescent manometer, allowing its use at extreme conditions of high pressure and temperature.

Due to the fact that the ^2E level is located below the $^4T_2$ state and that the usual kinetics from the ^2E level is much longer (~ms) than that of the $^4T_2$ level (~tens of μs), the luminescence decay profile of Mn^{4+} ions is dominated by the signal associated with the depopulation of the ^2E level. However, the ^2E and $^4T_2$ levels are coupled to each other by the spin-orbital interaction. This interaction shortens the lifetime of the ^2E level and increases the probability of its radiative depopulation. Therefore, when the applied pressure elevates the energy of the $^4T_2$ level, the spin-orbital coupling is weakened and thus the luminescence decay time is prolonged. This effect was used in the case of the $K_2Ge_4O_9$:0.1%Mn^{4+} material to develop a lifetime-based luminescence manometer. As can be clearly seen, an increase in isostatic pressure significantly affects the luminescence decay profile of Mn^{4+} ions by its elongation and more exponential course (Fig. 7a). The determined values of the average lifetime (τ_{avr}) increase monotonically from 0.97 ms at ambient pressure to 1.55 ms at 6 GPa (Fig. 7b). Above this value, a saturation of decay time values is observed. Quantitative analysis of the change in the lifetime of the ^2E level as a function of pressure done by determining relative sensitivity showed that the $S_{R,p}$ value increases from 4%/GPa at ambient conditions up to 12%/GPa at 3.3 GPa, and then decreases to 0.8%/GPa at 7.2 GPa (Fig. 7c). Notably, the effect observed for the Mn^{4+} emission kinetics is in contrast to manometers based on the luminescence kinetics of lanthanide-doped materials, where both the applied pressure and temperature cause the analogous direction of change (shortening or prolongation tendency) in excited state lifetime. To verify this hypothesis for the $K_2Ge_4O_9$:0.1%Mn^{4+} material, an analysis of the luminescence decay profile as a function of temperature in the range of 83–423 K was performed (Fig. 7d). Elevation of temperature results in a decrease in the τ_{avr} with a low quenching rate, up to around 350 K, above which point a sharp reduction in τ_{avr} value, down to 0.01 ms at 423 K, is recorded (Fig. 7e). This rapid effect observed above 350 K is caused by the depopulation of the ^2E level by thermalization of the $^4T_2$ state. Therefore, the relative thermal sensitivity below ≈350 K is

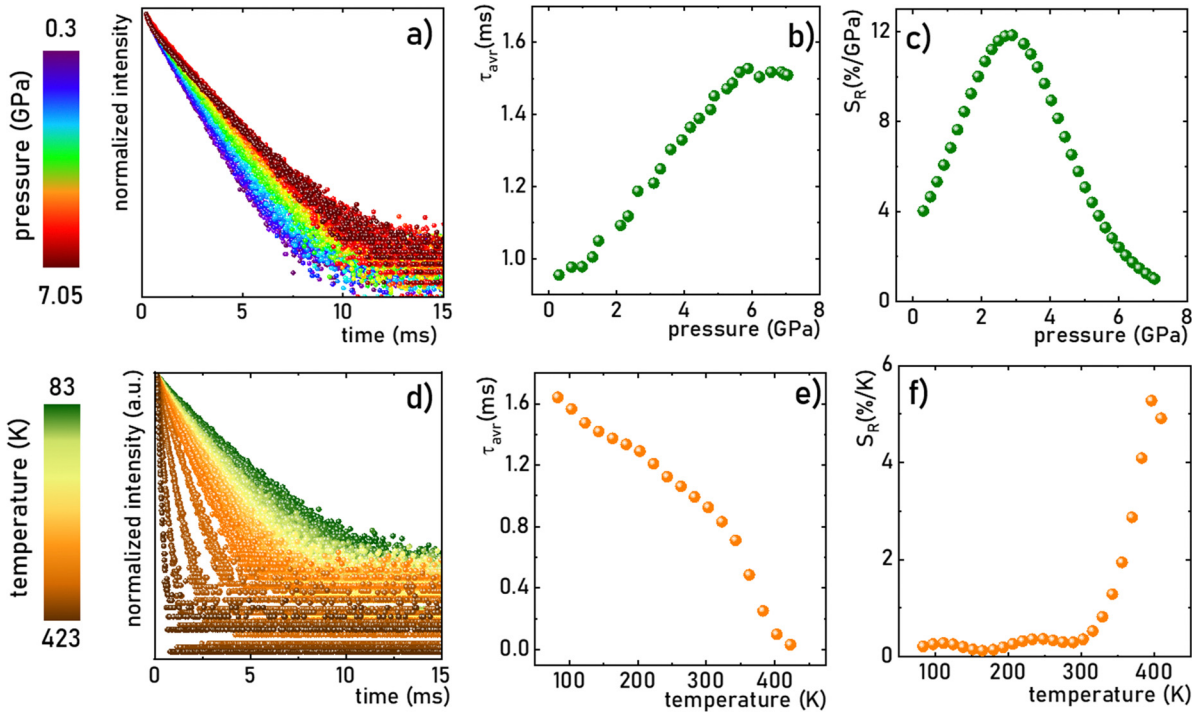

Fig. 7 The luminescence decay profile of the ^{2}E state in $K_2Ge_4O_9$:0.1%Mn^{4+} (λ_{exc} = 445 nm, λ_{em} = 651 nm) measured at room temperature as a function of applied pressure (a) and corresponding τ_{avr} (b) and S_R (c); the influence of the temperature on the luminescence decay profile of the ^{2}E state in $K_2Ge_4O_9$:0.1%Mn^{4+} (λ_{exc} = 445 nm, λ_{em} = 651 nm) at ambient pressure (d) and corresponding τ_{avr} (e) and S_R (f).

lower than 1%/K, and a further temperature increase enhances sensitivity value up to $S_{R,T}$ = 4%/K at around 423 K (Fig. 6f).

$$S_{R,p} = \frac{1}{\tau_{avr}} \frac{\Delta\tau_{avr}}{\Delta p} 100\% \quad (15)$$

$$S_{R,T} = \frac{1}{\tau_{avr}} \frac{\Delta\tau_{avr}}{\Delta T} 100\% \quad (16)$$

Although the determined maximum sensitivity of the lifetime-based luminescence manometer $K_2Ge_4O_9$:0.1%Mn^{4+}, *i.e.* S_R = 12%/GPa, is lower than the maximum value for the $Sr_4Al_{14}O_{25}$:Mn^{4+} (S_R = 35%/GPa at 0.8 GPa),[18] it should be noted that at higher pressure values (above 1.5 GPa) the relative sensitivity for $Sr_4Al_{14}O_{25}$:Mn^{4+} drops dramatically, and at 3.3 GPa is already much below 1%/GPa. In this pressure range of around 3 GPa, definitely more pronounced manometric performance is shown for $SrGdAlO_4$:Mn^{4+} with a relative sensitivity of S_R = 7.85%/GPa.[19] However, the value of S_R = 12%/GPa undoubtedly confirms the predominance of $K_2Ge_4O_9$:0.1%Mn^{4+} in this pressure range around 3 GPa confirming its significant application advantages. The performed comparison indicates that the sensitivity of the luminescent manometer based on the emission kinetics of Mn^{4+} ions is strongly affected by the composition host material. Therefore, the selection of a suitable phosphor for luminescence based pressure sensing should be dictated by the requirements imposed by the type of application.

Conclusion

In this work, the influence of applied pressure on the spectroscopic properties of $K_2Ge_4O_9$:Mn^{4+} crystals was investigated in order to develop a highly sensitive, multi-parameter luminescent manometer based on sensing in three different modes, namely, (I) the kinetics of the ^{2}E state of Mn^{4+}; (II) the emission line shift; and (III) LIR. The quenching of the luminescence intensity and shortening of the lifetime of the ^{2}E excited state with an increase of the Mn^{4+} concentration motivated the selection of 0.1% of Mn^{4+} as an optimal concentration of dopant ions for further experiments. The performed high-pressure studies of the spectroscopic properties of the $K_2Ge_4O_9$:0.1% Mn^{4+} material indicate that due to the nephelauxetic effect associated with the change in the covalency of the Mn^{4+}–O^{2-} bond, the energy of the $^2E \rightarrow {}^4A_2$ emission band decreases monotonically with a shift rate of 0.59 nm GPa^{-1} (12 cm^{-1} GPa^{-1}). However, the determined thermal dependence of the spectral position of the R line was relatively large, *i.e.* 0.02 nm K^{-1} (0.45 cm^{-1} K^{-1}). Above 3 GPa the intensity of the R line started to decrease with respect to the phonon progression lines, enabling the development of the ratiometric luminescence manometer operating in the 3–7.6 GPa *p*-range, with the maximal relative sensitivity of S_R = 21.7%/GPa at 5.9 GPa, and a TIMF factor of 5425 K GPa^{-1} at 300 K. Another effect associated with the applied pressure was the reduction of the spin–orbital coupling between ^{2}E and $^4T_2$ states, related to the enhancement of the energy of the $^4T_2$ state under structure compression. As a consequence, the luminescence decay profile

of the ^2E state of Mn^{4+} ions elongates and becomes more exponential with pressure. The monotonic prolongation of τ_{avr} in the 0.3–6 GPa *p*-range enables the development of a lifetime-based manometer, characterized by S_R max = 12%/GPa at 3 GPa. This is, to the best of our knowledge, the most sensitive lifetime-based luminescent manometer operating in the pressure range above 2 GPa reported so far. Additionally, the strong thermal susceptibility of the R-line of Mn^{4+} ions in $K_2Ge_4O_9$ (0.02 nm K^{-1}), together with its negligible pressure-induced shift in the low pressure regime, enables the application of this phosphor as a bi-functional pressure–temperature sensor, in both scientific and industrial applications.

Conflicts of interest

There are no conflicts to declare.

Acknowledgements

This work was supported by the National Science Center (NCN) Poland under project no. DEC-UMO-2020/37/B/ST5/00164. W. M. P. acknowledges the support from the Foundation for Polish Science (FNP) under the START programme.

References

1 X. D. Wang, O. S. Wolfbeis and R. J. Meier, *Chem. Soc. Rev.*, 2013, **42**, 7834–7869.
2 C. D. S. Brites, A. Millán and L. D. Carlos, in *Handbook on the Physics and Chemistry of Rare Earths*, ed. B. Jean-Claude and P. B. T.-H. Vitalij, Elsevier, 2016, vol. 49, pp. 339–427.
3 F. Vetrone, R. Naccache, A. Zamarrón, A. J. De La Fuente, F. Sanz-Rodríguez, L. M. Maestro, E. M. Rodriguez, D. Jaque, J. G. Sole and J. A. Capobianco, *ACS Nano*, 2010, **4**, 3254–3258.
4 L. Marciniak, K. Kniec, K. Elżbieciak-Piecka, K. Trejgis, J. Stefanska and M. Dramićanin, *Coord. Chem. Rev.*, 2022, **469**, 214671.
5 J. Zhou, B. del Rosal, D. Jaque, S. Uchiyama and D. Jin, *Nat. Methods*, 2020, **17**, 967–980.
6 M. Back, J. Ueda, H. Hua and S. Tanabe, *Chem. Mater.*, 2021, **33**, 3379–3385.
7 U. R. Rodríguez-Mendoza, S. F. León-Luis, J. E. Muñoz-Santiuste, D. Jaque and V. Lavín, *J. Appl. Phys.*, 2013, **113**, 213517.
8 J. D. Barnett, S. Block and G. J. Piermarini, *Rev. Sci. Instrum.*, 1973, **44**, 1–9.
9 M. Runowski, P. Wozny, N. Stopikowska, I. R. Martín, V. Lavín and S. Lis, *ACS Appl. Mater. Interfaces*, 2020, **12**, 43933–43941.
10 A. Bednarkiewicz, L. Marciniak, L. D. Carlos and D. Jaque, *Nanoscale*, 2020, **12**, 14405–14421.
11 L. Labrador-Páez, M. Pedroni, A. Speghini, J. García-Solé, P. Haro-González and D. Jaque, *Nanoscale*, 2018, **10**, 22319–22328.
12 C. D. S. Brites, S. Balabhadra and L. D. Carlos, *Adv. Opt. Mater.*, 2019, **7**, 1801239.
13 W. Piotrowski, M. Kuchowicz, M. Dramićanin and L. Marciniak, *Chem. Eng. J.*, 2021, **428**, 131165.
14 M. D. Dramićanin, *J. Appl. Phys.*, 2020, **128**, 40902.
15 W. Becker, *J. Microsc.*, 2012, **247**, 119–136.
16 P. Zhou, Q. Zhang, F. Peng, B. Sun, X. Dou, B. Liu, D. Han, Y. Xue and K. Ding, *J. Rare Earths*, 2022, **40**, 870–877.
17 M. Runowski, J. Marciniak, T. Grzyb, D. Przybylska, A. Shyichuk, B. Barszcz, A. Katrusiak and S. Lis, *Nanoscale*, 2017, **9**, 16030–16037.
18 M. Pieprz, W. Piotrowski, P. Woźny, M. Runowski and L. Marciniak, *Adv. Opt. Mater.*, 2023, 2301316.
19 M. Pieprz, M. Runowski, P. Woźny, J. Xue and L. Marciniak, *J. Mater. Chem. C*, 2023, **11**, 11353–11360.
20 M. Tian, Y. Gao, P. Zhou, K. Chi, Y. Zhang and B. Liu, *Phys. Chem. Chem. Phys.*, 2021, **23**, 20567–20573.
21 Y. Masubuchi, S. Nishitani, S. Miyazaki, H. Hua, J. Ueda, M. Higuchi and S. Tanabe, *Appl. Phys. Express*, 2020, **13**, 42009.
22 M. Runowski, A. Shyichuk, A. Tymiński, T. Grzyb, V. Lavín and S. Lis, *ACS Appl. Mater. Interfaces*, 2018, **10**, 17269–17279.
23 M. Runowski, in *Handbook of Nanomaterials in Analytical Chemistry: Modern Trends in Analysis*, ed. C. Mustansar Hussain, Elsevier, 2019, pp. 227–273.
24 H. Y. Wong, X. Le Zhou, C. T. Yeung, W. L. Man, P. Woźny, A. Półrolniczak, A. Katrusiak, M. Runowski and G. L. Law, *Chem. Eng. J. Adv.*, 2022, **11**, 100326.
25 M. Behrendt, K. Szczodrowski, S. Mahlik and M. Grinberg, *Opt. Mater.*, 2014, **36**, 1616–1621.
26 S. Mahlik, M. Behrendt, M. Grinberg, E. Cavalli and M. Bettinelli, *Opt. Mater.*, 2012, **34**, 2012–2016.
27 S. Mahlik, M. Grinberg, E. Cavalli, M. Bettinelli and P. Boutinaud, *J. Phys.: Condens. Matter*, 2009, **21**, 105401.
28 A. D. Lozano-Gorrín, U. R. Rodríguez-Mendoza, V. Venkatramu, V. Monteseguro, M. A. Hernández-Rodríguez, I. R. Martín and V. Lavín, *Opt. Mater.*, 2018, **84**, 46–51.
29 M. Szymczak, M. Runowski, V. Lavín and L. Marciniak, *Laser Photonics Rev.*, 2023, **17**, 2200801.
30 M. Szymczak, M. Runowski, M. G. Brik and L. Marciniak, *Chem. Eng. J.*, 2023, **466**, 143130.
31 M. Szymczak, P. Woźny, M. Runowski, M. Pieprz, V. Lavín and L. Marciniak, *Chem. Eng. J.*, 2023, **453**, 139632.
32 Q. Zeng, M. Runowski, J. Xue, L. Luo, L. Marciniak, V. Lavín and P. Du, *Adv. Sci.*, 2023, 2308221.
33 X. Ding, Q. Wang and Y. Wang, *Phys. Chem. Chem. Phys.*, 2016, **18**, 8088–8097.
34 M. Cheng, X.-X. Wu and W.-C. Zheng, *Optik*, 2018, **156**, 459–462.
35 P. Li, L. Wondraczek, M. Peng and Q. Zhang, *J. Am. Ceram. Soc.*, 2016, **99**, 3376–3381.
36 R. Oka, D. Nishi and T. Hayakawa, *Phys. Status Solidi*, 2022, **259**, 2100615.
37 G. J. Redhammer and G. Tippelt, *Acta Crystallogr., Sect. C: Cryst. Struct. Commun.*, 2013, **69**, 995–1001.
38 M. G. Brik, C. G. Ma, A. M. Srivastava and M. Piasecki, *Chin. J. Lumin.*, 2020, **41**, 1011–1029.

39 D. Chen, Y. Zhou, W. Xu, J. Zhong, Z. Ji and W. Xiang, *J. Mater. Chem. C*, 2016, **4**, 1704–1712.
40 J. Xu, J. Ueda and S. Tanabe, *J. Am. Ceram. Soc.*, 2017, **100**, 4033–4044.
41 S. Adachi, *ECS J. Solid State Sci. Technol.*, 2020, **9**, 016001.
42 M. Medić, Z. Ristić, S. Kuzman, V. Đorđević, I. Vukoje, M. G. Brik and M. D. Dramićanin, *J. Lumin.*, 2020, **228**, 117646.
43 M. G. Brik, N. M. Avram and C. N. Avram, in *Optical Properties of 3d-Ions in Crystals: Spectroscopy and Crystal Field Analysis*, ed. N. M. Avram and M. G. Brik, Springer Berlin Heidelberg, Berlin, Heidelberg, 2013, vol. 9783642308, pp. 29–94.
44 A. M. Srivastava and M. G. Brik, *Opt. Mater.*, 2013, **35**, 1544–1548.
45 C. G. Ma, Y. Wang, D. X. Liu, Z. Li, X. K. Hu, Y. Tian, M. G. Brik and A. M. Srivastava, *J. Lumin.*, 2018, **197**, 142–146.
46 R. A. Forman, G. J. Piermarini, J. Dean Barnett and S. Block, *Science*, 1972, **176**, 284–285.
47 A. V. Romanenko, S. V. Rashchenko, A. Kurnosov, L. Dubrovinsky, S. V. Goryainov, A. Y. Likhacheva and K. D. Litasov, *J. Appl. Phys.*, 2018, **124**, 165902.
48 G. J. Piermarini, S. Block, J. D. Barnett and R. A. Forman, *J. Appl. Phys.*, 1975, **46**, 2774–2780.
49 T. Zheng, L. Luo, P. Du, S. Lis, U. R. Rodríguez-Mendoza, V. Lavín and M. Runowski, *Chem. Eng. J.*, 2022, **446**, 136839.